STATE RESEARCH CENTER OF RUSSIA
INSTITUTE FOR HIGH ENERGY PHYSICS
142281, Protvino, Moscow Region, Russia

NuMI–B–XXX
April 30, 2002

Technical Design of the Target Pile Protection Baffle

(Task B Report of the Accord between FNAL and IHEP)

S.Filippov, V.Garkusha, R.Gibadullin*, F.Novoskoltsev,
I.Ponimash*, T.Ryabova, V.Zarucheisky

*) Institute of Physics and Power Engineering, Obninsk, Kaluga region, Russia

Contents

1 Introduction **3**

2 Choice of the Baffle Length **4**
2.1 Temperature and Stresses in the Cooling Pipe Steel 5
2.2 Temperature and Stresses in the Horn Neck 5
2.3 Temperature and Stresses in the Ceramic Insulator 6

3 Choice of the Baffle Length (cont.) **8**

4 Baffle Design **20**

5 Normal Operational Mode **24**
5.1 Convection Coefficients for the Air Cooling of Baffle 24
5.2 Baffle Temperature 24

6 Emergency Mode **28**
6.1 Maximum Baffle Temperature 28
6.2 Temperature Monitoring 28
6.3 Stresses in the Baffle 29

7 Conclusions **34**

1 Introduction

The function of the baffle collimator is to protect the target and horns against the failure from the primary proton beam. Taking into account an influence of baffle on the neutrino spectra at the nominal sizes of proton beam, the diameter of hole for a proton beam passage is chosen equal to 10 mm. The transverse size of baffle should be large enough to overlap the possible trajectories of mis-steered proton beam, which lie outside this area, whereas the length of baffle should be sufficient to decrease the energy deposition density (or temperature rise) induced by this beam in some units of target and horn designs to provide their safe operation. The function of baffle defines its two operational modes:

- the normal operation mode, when the proton beam passes through the hole towards the target, hitting the baffle only by its tail. The 1% of a primary beam intensity was supposed in a beam tail for calculations of baffle temperature in the normal operation mode, which determines the way of baffle cooling;

- the emergency mode, when the mis-steered proton beam of full intensity strikes the face of baffle. Besides the length and transverse size of baffle, the emergency mode determines some other technical aspects of a baffle design, i.e. a system of thermocouples for monitoring of baffle temperature with the aim to detect an emergency situation and, probably, to align the baffle with respect to proton beam.

The choice of baffle length, which was based on calculations of an energy deposition density in some specific parts of target and horn designs, is given in **Sections 2** and **3** for two different positions of baffle with respect to the target. **Section 4** presents the description of baffle design. Results of temperature and stress calculations for two operational modes of baffle are given in **Sections 5** and **6**.

To verify the reality of the full-size baffle construction, the 45 cm length prototype was produced using the construction technique proposed in this Report for baffle collimator. The photos of prototype, as well as some general conclusions regarding considered baffle design are given in **Section 7**.

2 Choice of the Baffle Length

The main parameter, which governs the choice of the baffle length, is the energy deposition density induced in some units of target and horn designs by the mis-steered proton beam hitting the baffle. The weakest points of these designs are:

- cooling pipes of a target;
- the horn neck;
- the metal-ceramic adapter (insulator), used for insulation of the target casing from the ground.

Calculations of the energy deposition density were made using the IHEP version of MARS [1] for three lengths of the baffle: 40 cm, 80 cm and 120 cm. It was assumed that the 70 mm diameter baffle with the 10 mm diameter hole is made from the ZXF-5Q graphite grade of the Poco Graphite Inc.[1] In all these cases the downstream end of the baffle was located $L_{bt} = 176$ cm upstream the target core (i.e. about 2 m upstream the horn).

Results of calculations showed, that the essentially non-uniform, local heating of some units of target and horn designs are caused by the passage through this unit of non-interacting with baffle protons. Therefore, calculations were made for the following directions of the mis-steered proton beam, as it is shown in Figure 2.1. Direction 1 of the non-interacting proton beam hits the 0.3 mm thick wall of cooling pipe at the point where it is soldered to graphite segments. Direction 2 of the non-interacting proton beam hits the horn neck so that the radius of the proton beam axis is equal to the average radius of the neck. Directions 3 and 4 of non-interacting protons hit the ceramic insulator.

To simplify ANSYS calculations and thus to obtain quickly the estimate of thermal stresses, the two-dimensional approach was used under two different boundary conditions:

- *the plane stress*, when the ends of units are free to move in the longitudinal direction, i.e. $\varepsilon_(zz) \neq 0$, where ε_{zz} is the longitudinal deformation;
- *the plane strain*, when the ends of unit are constrained, i.e. $\varepsilon_{zz} = 0$.

[1] The same graphite grade was considered as a possible material for both LE and ME NuMI targets [2].

2.1 Temperature and Stresses in the Cooling Pipe Steel

The maximum density of an energy deposition in the cooling pipe steel and corresponding temperature rise as functions of the baffle length are shown in Figure 2.2. An increase of the baffle length from 40 cm to 120 cm decreases the temperature rise in steel from 157°C to 25°C.

The evolution in time of circumferential stresses $S_{\varphi\varphi}$ in two diametrically opposite points of a cooling pipe is shown in Figure 2.3a for the baffle length of 40 cm and the plane stress boundary condition. The stresses are essentially dynamical, because the value of $v_s\tau \simeq 47$ mm is of the same order of magnitude as $2\pi r = 19$ mm, where v_s is the sound velocity in the steel, τ is the beam spill duration and r is the radius of a cooling pipe. The stress in point 1 reaches its maximum of 54 MPa in 24 μs after beginning of a beam pulse.

Results of calculations under the plane strain boundary condition show that the stress in the steel pipe is defined mainly by S_{zz}, which arises besides of circumferential stress $S_{\varphi\varphi}$ due to $\varepsilon_{zz} = 0$. In this case $S_{eq} \simeq |S_{zz}| \gg |S_{\varphi\varphi}|$.

Maximum stresses in point 1 as functions of the baffle length calculated under two different boundary conditions are shown in Figure 2.3b. It is necessary to note, that the real value of stress resides somewhere between these two plots, and that even at the baffle length of 80 cm the maximum stress is essentially lower than the yield strength of the CT852 steel (340 MPa), used for construction of cooling pipes [2].

In case of the 40 cm length baffle the maximum density of an energy deposition in a cooling water is equal to 25 J/cm^3. It gives the 6°C water temperature rise, which may be neglected with respect to the temperature of a cooling water in the normal operation mode.

2.2 Temperature and Stresses in the Horn Neck

The maximum density of an energy deposition in the horn neck varies from 185 J/cm^3 at the 40 cm length baffle up to 20.4 J/cm^3 at the 120 cm one. The corresponding temperature rise decreases from 76°C to 8.4°C (Figure 2.4). One should note, that calculations of the energy deposition in the horn neck for the normal operation mode (when the primary beam hits the axis of target) give the uniformly distributed value of 22.5 J/cm^3.

Calculations of stresses in the horn neck in case of its local heating by the non-interacting proton beam is a rather complicated task, because it

should take also into account the magnetic pressure, the thermal stresses due to the Joule heat load and the interference of these stresses with the thermal stress due to the beam heating.

Results of ANSYS calculations of thermal stresses in the horn neck caused by only the non-interacting proton beam in case of the 120 cm length baffle are shown in Figure 2.5. Similar to steel cooling pipes, the stresses are essentially dynamical.

To estimate the total stress in the horn neck, we suppose that there are only two stresses in the neck at the normal operation conditions, i.e. circumferential $S_{\varphi\varphi}$ and axial S_{zz}, and the maximum von Mises stress (which occurs just after the beam pulse) is $S_{eq} \simeq 40$ MPa [3]. Simple estimation shows that the circumferential stress $S_{\varphi\varphi}$ due to the magnetic pressure is about 10 MPa. Then the axial stress may be estimated as $S_{zz} = \sqrt{2S_{eq}^2 - S_{\varphi\varphi}^2} \simeq 56$ MPa. From Figure 2.5 (bottom plots) one can get $S_{zz}^p \simeq 30$ MPa, $S_{\varphi\varphi}^p \simeq 12$ MPa and $S_{rr}^p \simeq 48$ MPa. The superscript index "p" means that the stress is caused by the non-interacting proton beam. Then in the worst case the total von Mises stress is:

$$S_{eq}^t = \frac{1}{\sqrt{2}}\sqrt{(|S_{zz}| + |S_{zz)}^p|)^2 + (|S_{\varphi\varphi}| + |S_{\varphi\varphi}^p|)^2 + (S_{rr}^p)^2}.$$

Substitution of given above values in this expression gives $S_{eq}^t \simeq 70$ MPa. This value is three times lower than the yield strength of an aluminum alloy 6061-T6 ($\sim$230 MPa at 100°C).

We note that at the baffle length of 80 cm the temperature rise is three times higher than for the 120 cm length baffle (Figure 2.4), and one may expect the total stress which is rather closed to the yield stress of the 6061-T6 alloy. Therefore, to provide a sufficient safety factor it is reasonable to choose the length of baffle equal to 120 cm.

2.3 Temperature and Stresses in the Ceramic Insulator

The metal-ceramic adapter (ceramic insulator), which is used for insulation of the target casing from the ground, consists of a hollow ceramic cylinder with two brazed kovar pipes. A hollow cylinder is machined out from the high frequency, vacuum tight ceramic BK94-1 (Russian grade). It is a high alumina ceramic consisting of Al_2O_3 to the extent of 94.4%. Properties of the BK94-1 ceramic are listed in Table 2.1.

Density, g/cm^3	3.65
Modulus of elasticity, GPa	270-295
Ultimate tensile strength, MPa	170-240
Ultimate compressive strength, GPa	2-3
Flexural strength, MPa	310-340
Coeff. of thermal expansion at 25-200°C, 10^{-6}1/K	5.7-6.67
Heat capacity, J/kg·K	800
Thermal conductivity, W/m·K	19-22
Maximum working temperature in air, °C	1600-1700

Table 2.1: Thermo-mechanical properties of the BK94-1 ceramic.

The maximum density of energy deposition decreases from 380 J/cm^3 at the baffle length of 40 cm to 66 J/cm^3 at the baffle length of 120 cm. The corresponding temperature rise varies from 130°C to 22.4°C (Figure 2.6). Because the primary proton beam has an elliptical spot size ($\sigma_x \times \sigma_y = 0.7 \times 1.4$ mm^2), thermal stresses are expected to be different for two directions of a proton beam (3 and 4).

Results of ANSYS calculations of stresses in the ceramic insulator (time evolution of stresses) for the 40 cm length baffle in case of the proton beam direction 3 are shown in Figures 2.7 and 2.8 for the plane stress and plane strain, respectively. In both cases of boundary conditions there is the compression of material in the center of a beam spot and the stretching of material on the internal surface of the ceramic cylinder (see also Figure 2.9).

Since the ultimate tensile strength of used ceramic is essentially smaller than its compressive strength (Table 2.1), the integrity of a ceramic cylinder will be defined by the value of stress on its internal surface. As it follows from given above results, even for the 40 cm length baffle, the tensile stress on the internal surface of the ceramic cylinder is not exceed the ultimate tensile strength of material. But to obtain the sufficient safety factor it is reasonable to use the longer baffle.

The tensile stresses on the internal surface of the ceramic cylinder as functions of the baffle length are given in Figure 2.10 for two different directions (3 and 4) of a primary proton beam. One can see that the values of stresses are almost the same for both considered proton beam directions and an increase of the baffle length up to 120 cm allows to decrease the tensile stress to 25 MPa.

3 Choice of the Baffle Length (cont.)

To increase the range of LE target motion (this allows to change the neutrino beam in a wider range of energies), it was decided to mount the baffle and target together minimum distance apart. As a consequence of new initial conditions, calculations of the energy deposition density were repeated for a new position of baffle when the downstream end of the baffle is located $L_{bt} = 86$ cm upstream the target core (i.e. about 1.1 m upstream the horn).

Three lengths of the baffle were considered at this stage of its study: 80, 120 and 160 cm. Besides of the steel cooling pipe, horn neck and ceramic insulator, calculations were made also for the solder joint between target segments and cooling pipes. Results of calculations in terms of a temperature rise are given in Figure 3.1. As it follows from these results:

1) The shift of baffle 90 cm closely to the target core leads to increasing of an energy deposition density and, correspondingly, temperature rise in all considered units of target and horn designs (see Figures 3.1a–3.1c). To compensate this increase of a temperature, the length of baffle should be increased at ~15 cm (from 120 cm up to 135 cm). Table 3.1 gives the comparison of temperature rises between two variants of baffle.

2) At the baffle length of 135 cm the temperature rise in the solder is equal to 64°C (Figure 3.1d), that is essentially lower than the melting temperature of soldered joint. For the used soft solder (85%Sn, 8%Zn, 7%Ag) this temperature is equal to 340°C.

Baffle length/position	steel pipe	horn neck	ceramic ins.	solder
120 cm/$L_{bt} = 176$ cm	25	8.4	21	–
135 cm/$L_{bt} = 86$ cm	33	10.0	27	64

Table 3.1: Temperature rises (°C) in some units of target and horn designs for two different lengths/positions of baffle.

In conclusion to Sections 2 and 3 one should note, that given above results were obtained assuming a short-term load (a few pulses) of the target and horn by the mis-steered primary proton beam, which hits the baffle collimator. Under these conditions the baffle with a length of 120 cm at $L_{bt} = 176$ cm (or 135 cm at $L_{bt} = 86$ cm) will provides a quite reliable protection from failure in case of the mis-steered proton beam even for the weakest parts of target and horn.

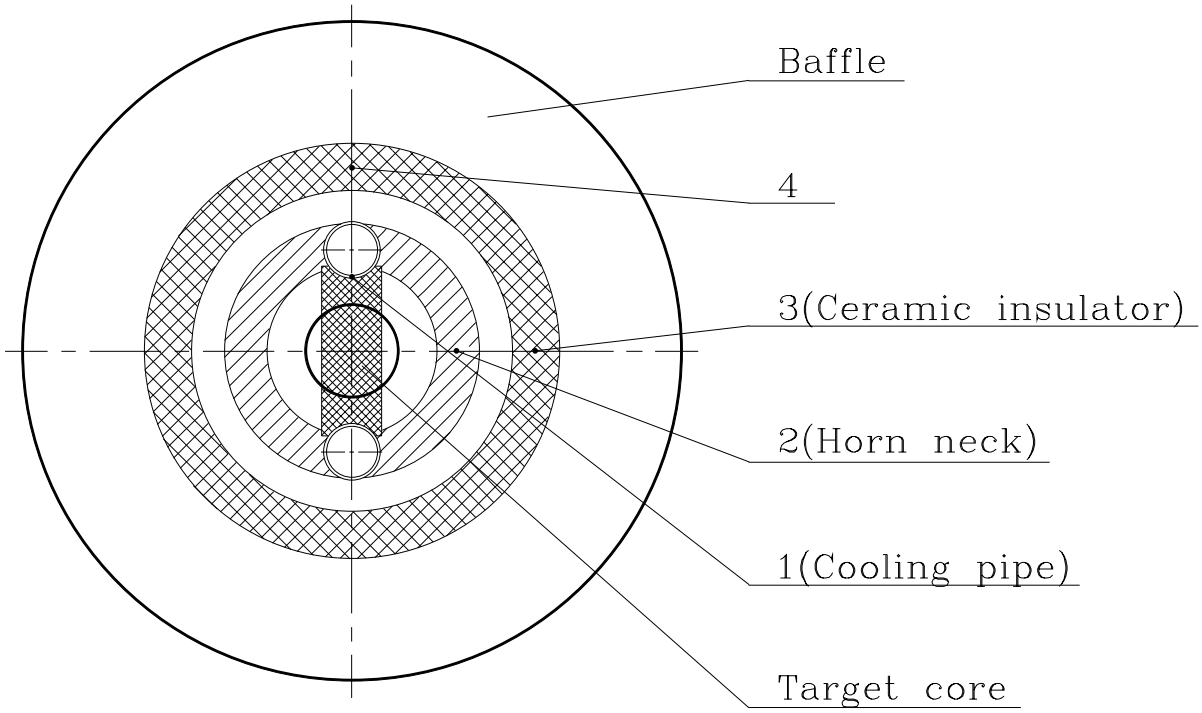

Figure 2.1: Projections of cooling pipes, horn neck and ceramic insulator onto the 70 mm diameter baffle collimator with the 10 mm diameter hole. Numbers 1÷4 marks positions of the mis-steered primary proton beam in front of the baffle. In all cases the direction of proton beam is collinear with the target & horn axis.

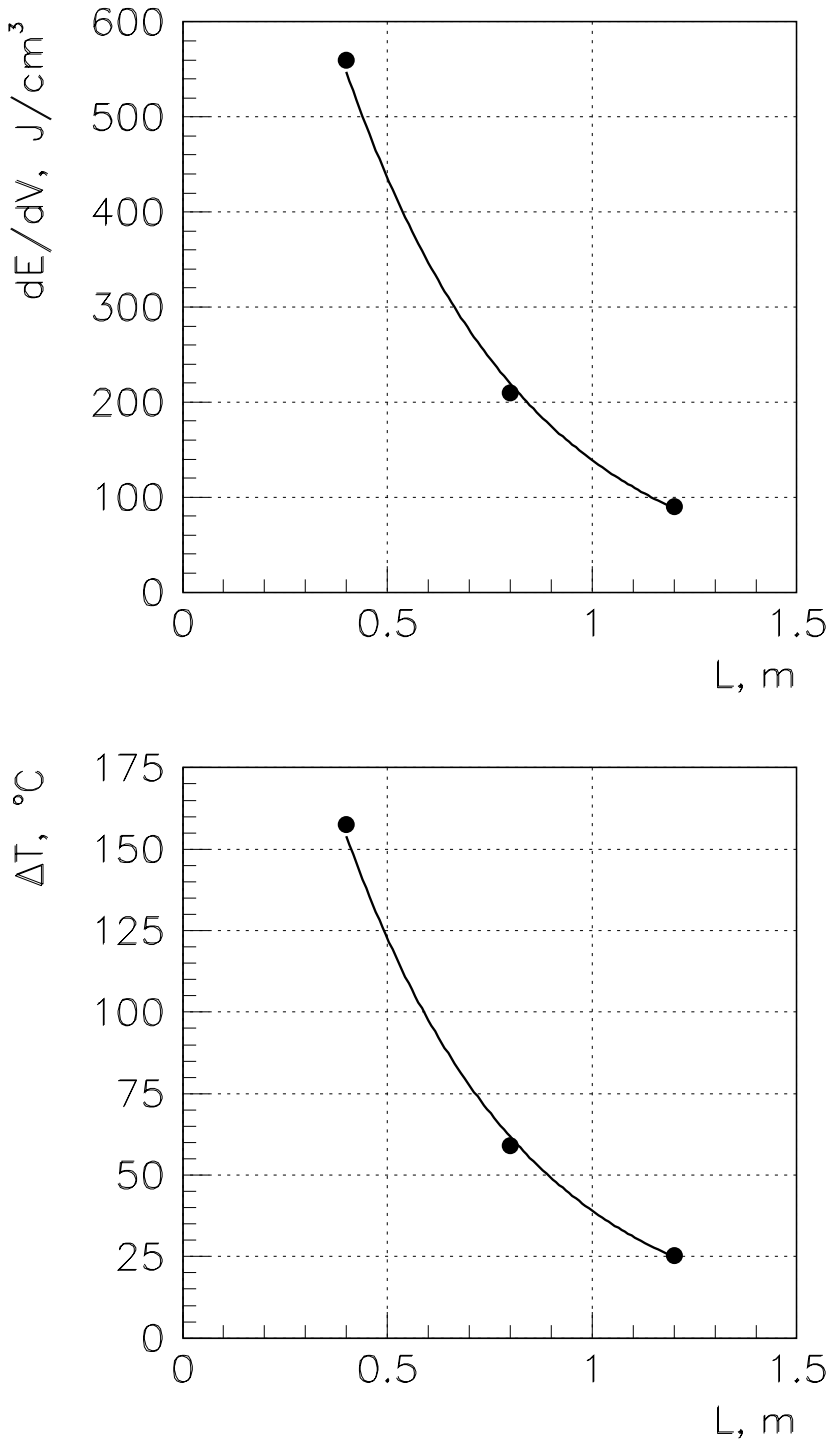

Figure 2.2: The maximum density of an energy deposition (top) and the temperature rise in the cooling pipe steel (bottom) for different lengths of the baffle in case of the proton beam direction 1.

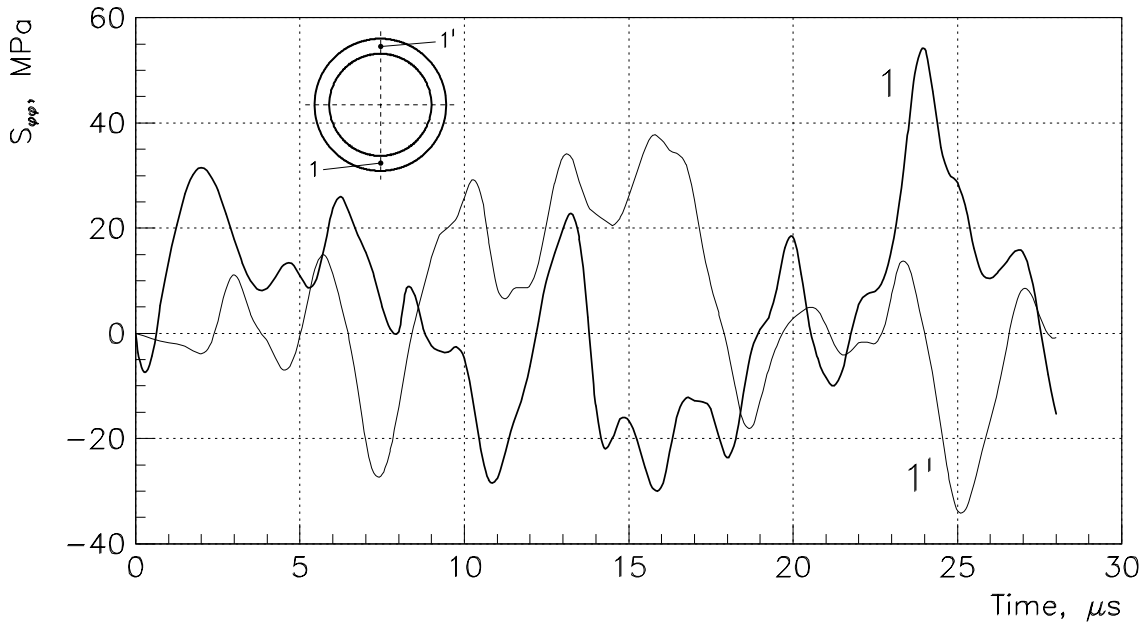

Figure 2.3a: Time evolution of circumferential stresses in two diametrically opposite points of a cooling pipe for the 40 cm length baffle.
Boundary conditions — the plane stress.

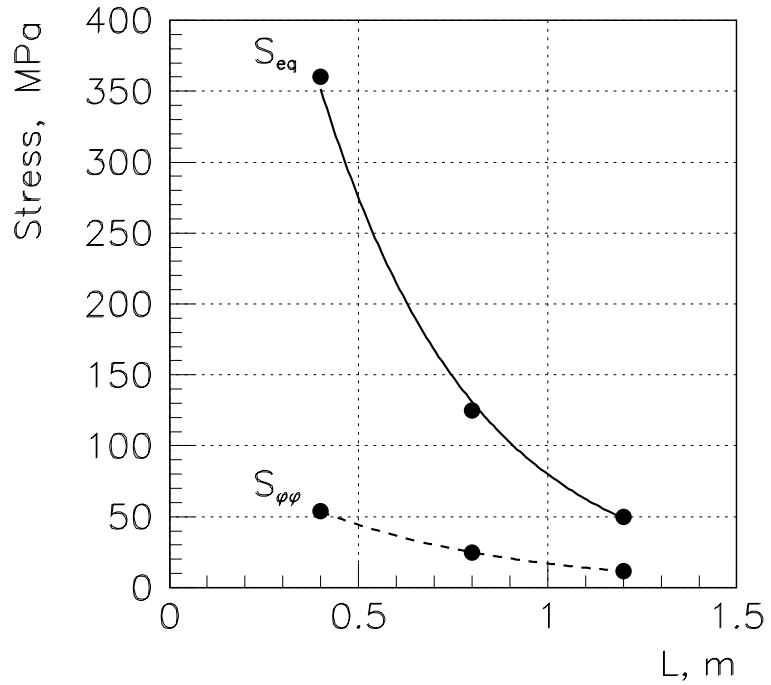

Figure 2.3b: Maximum values of stresses in a cooling pipe as functions of the baffle length. $S_{\varphi\varphi}$ — for the plane stress, S_{eq} — for the plane strain.

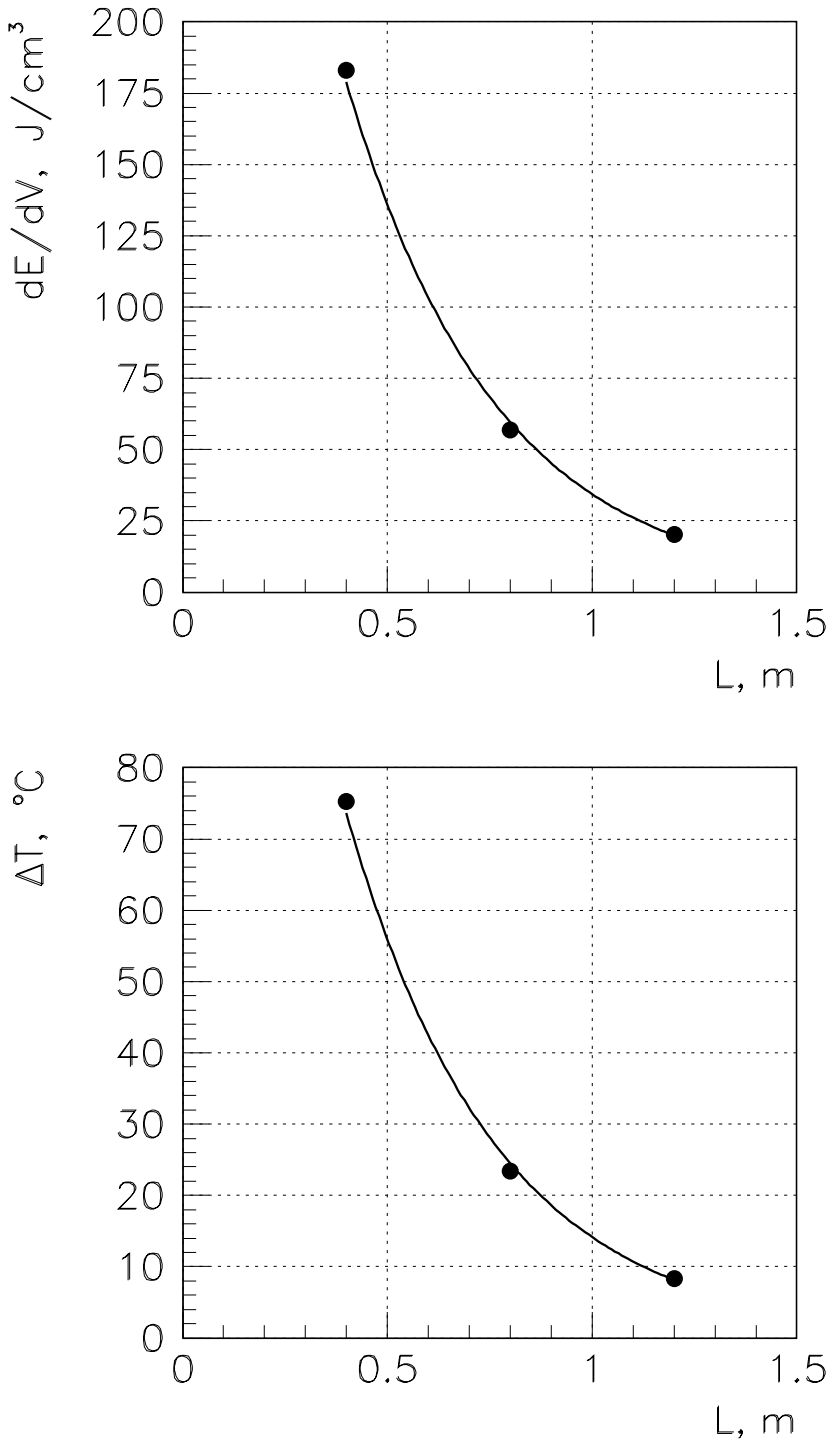

Figure 2.4: The maximum density of an energy deposition (top) and the temperature rise in the horn neck (bottom) for different lengths of the baffle in case of the proton beam direction 2.

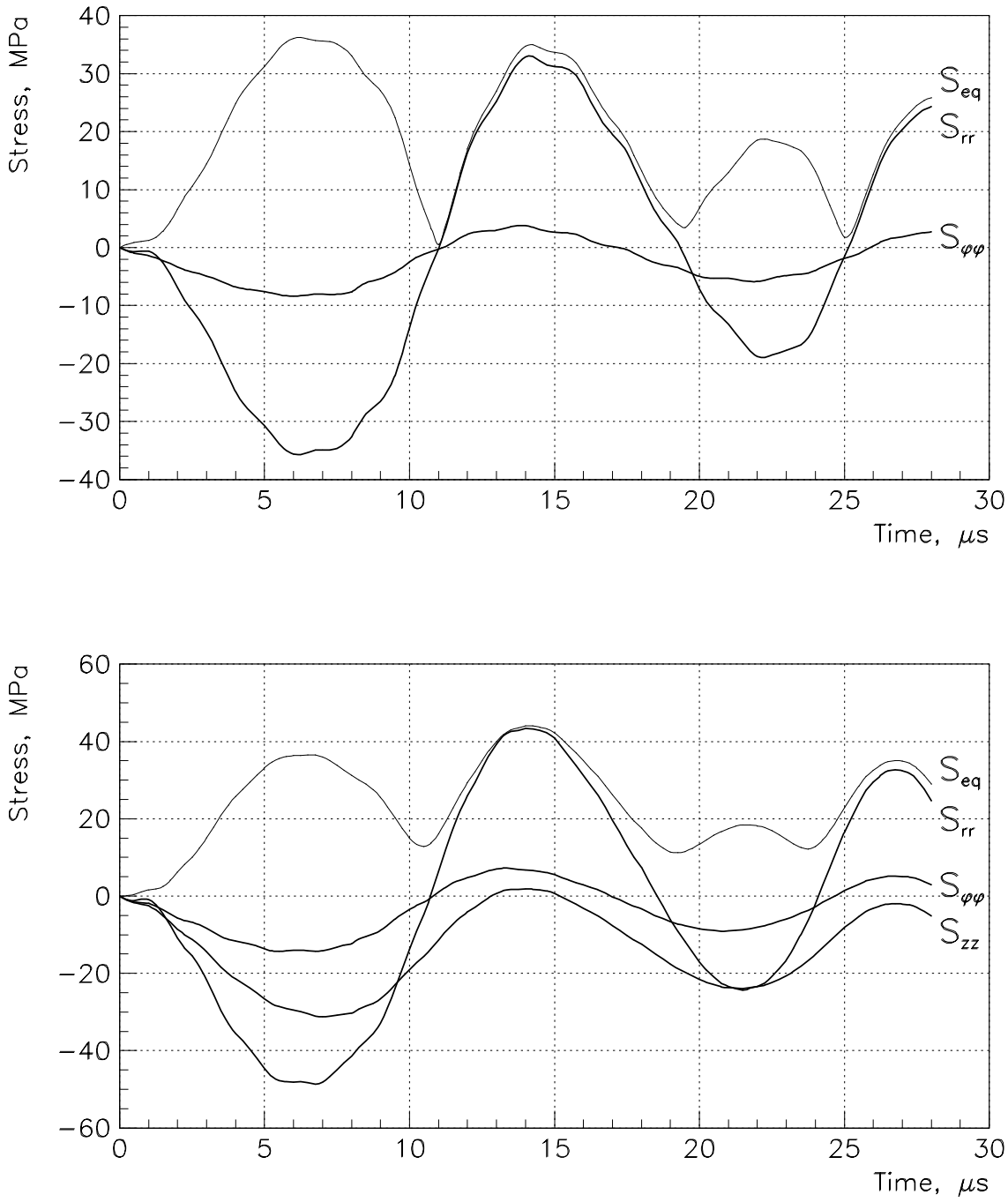

Figure 2.5: Time evolution of stresses in the horn neck in case of the proton beam direction 2 for the 120 cm length baffle. Boundary conditions — the plane stress (top) and the plane strain (bottom).

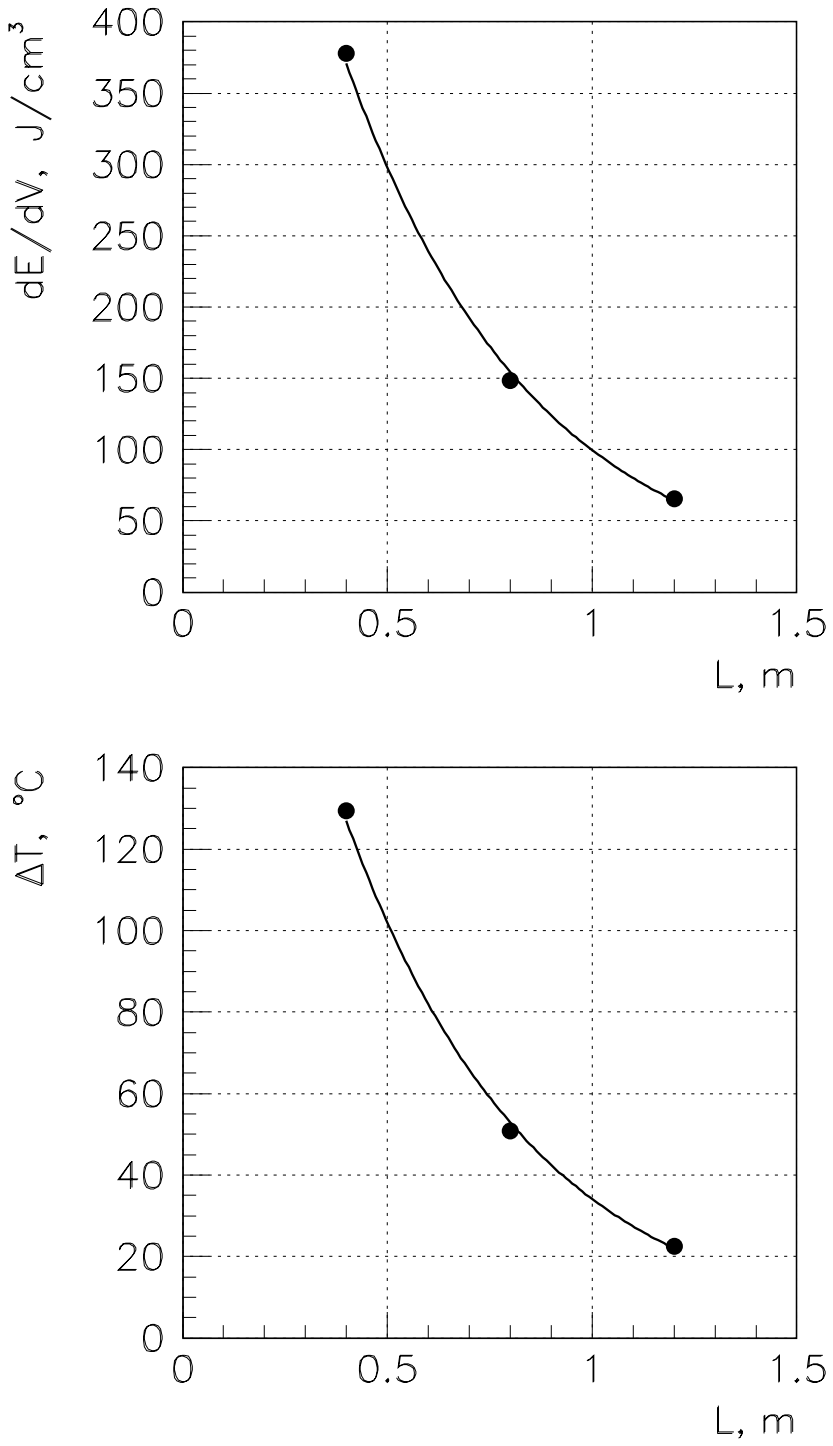

Figure 2.6: The maximum density of an energy deposition (top) and the temperature rise in the ceramic insulator (bottom) for different lengths of the baffle in case of the proton beam directions 3 and 4.

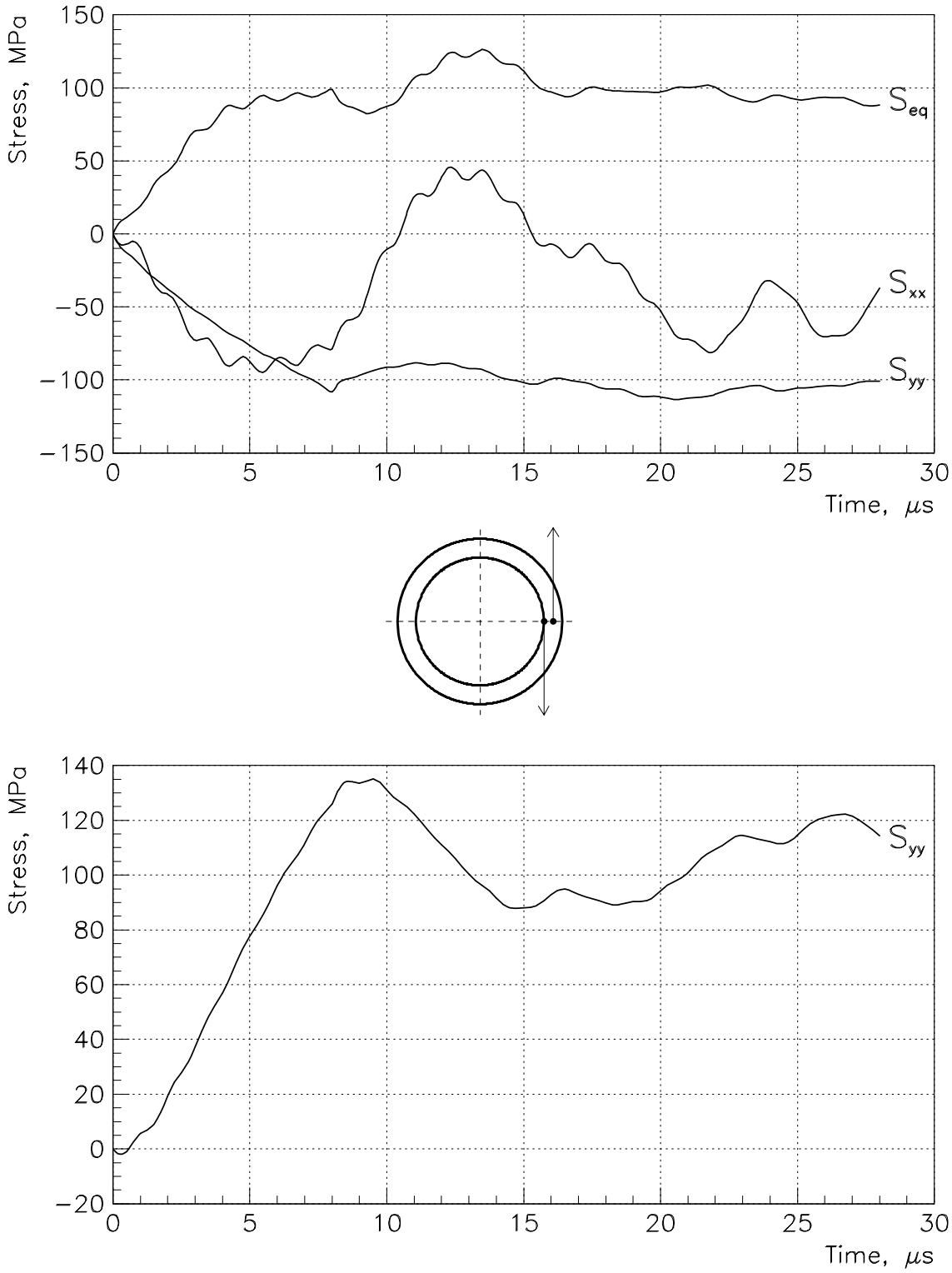

Figure 2.7: Time evolution of stresses at two points of the ceramic insulator in case of the proton beam direction 3 for the 40 cm length baffle. Boundary conditions — the plane stress.

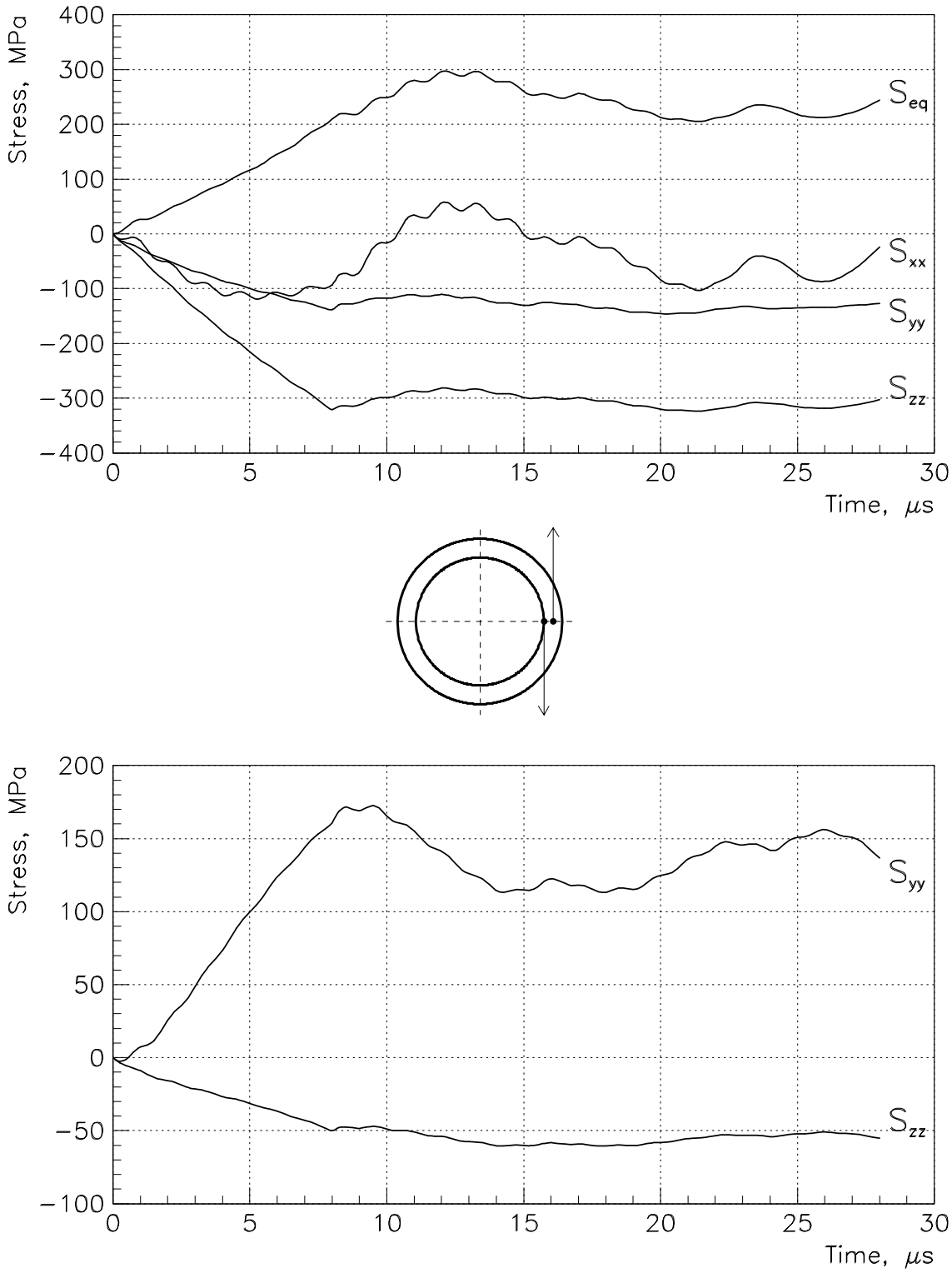

Figure 2.8: Time evolution of stresses at two points of the ceramic insulator in case of the proton beam direction 3 for the 40 cm length baffle. Boundary conditions — the plane strain.

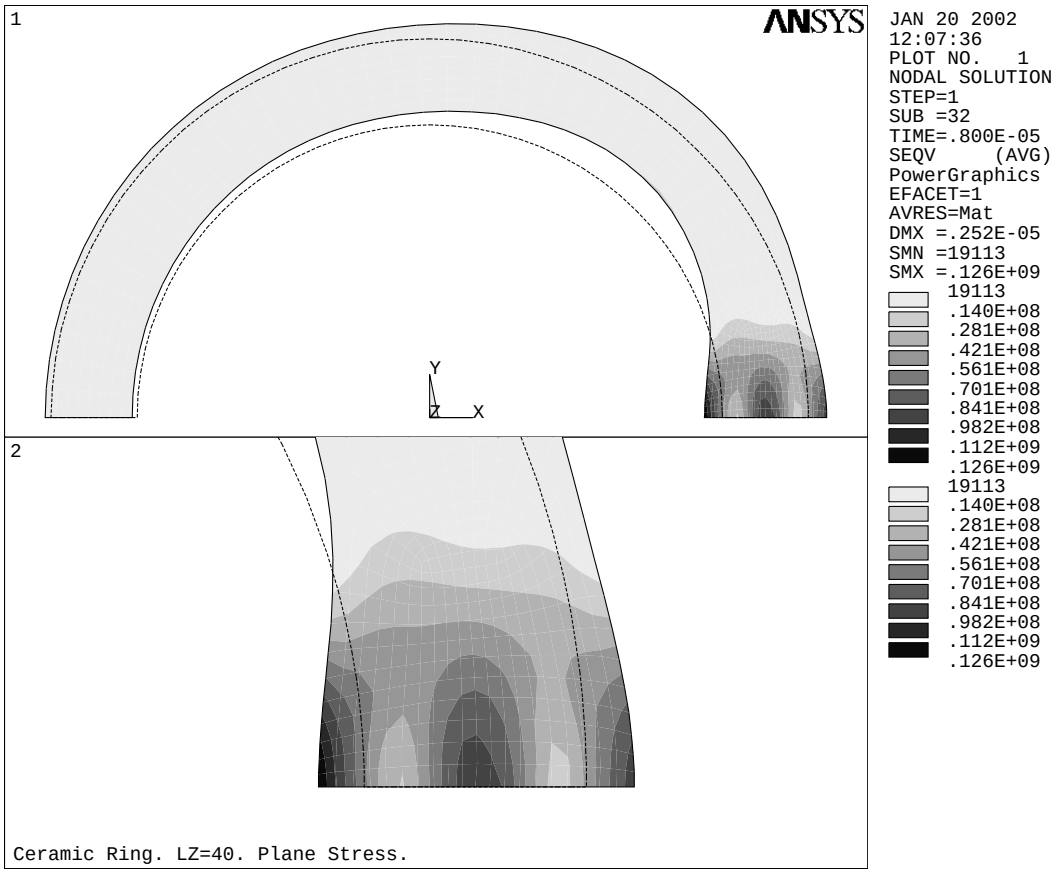

Figure 2.9: Distribution of the von Mises equivalent stress in the ceramic insulator after the beam spill in case of the proton beam direction 3 for the 40 cm length baffle. Boundary conditions — the plane stress.

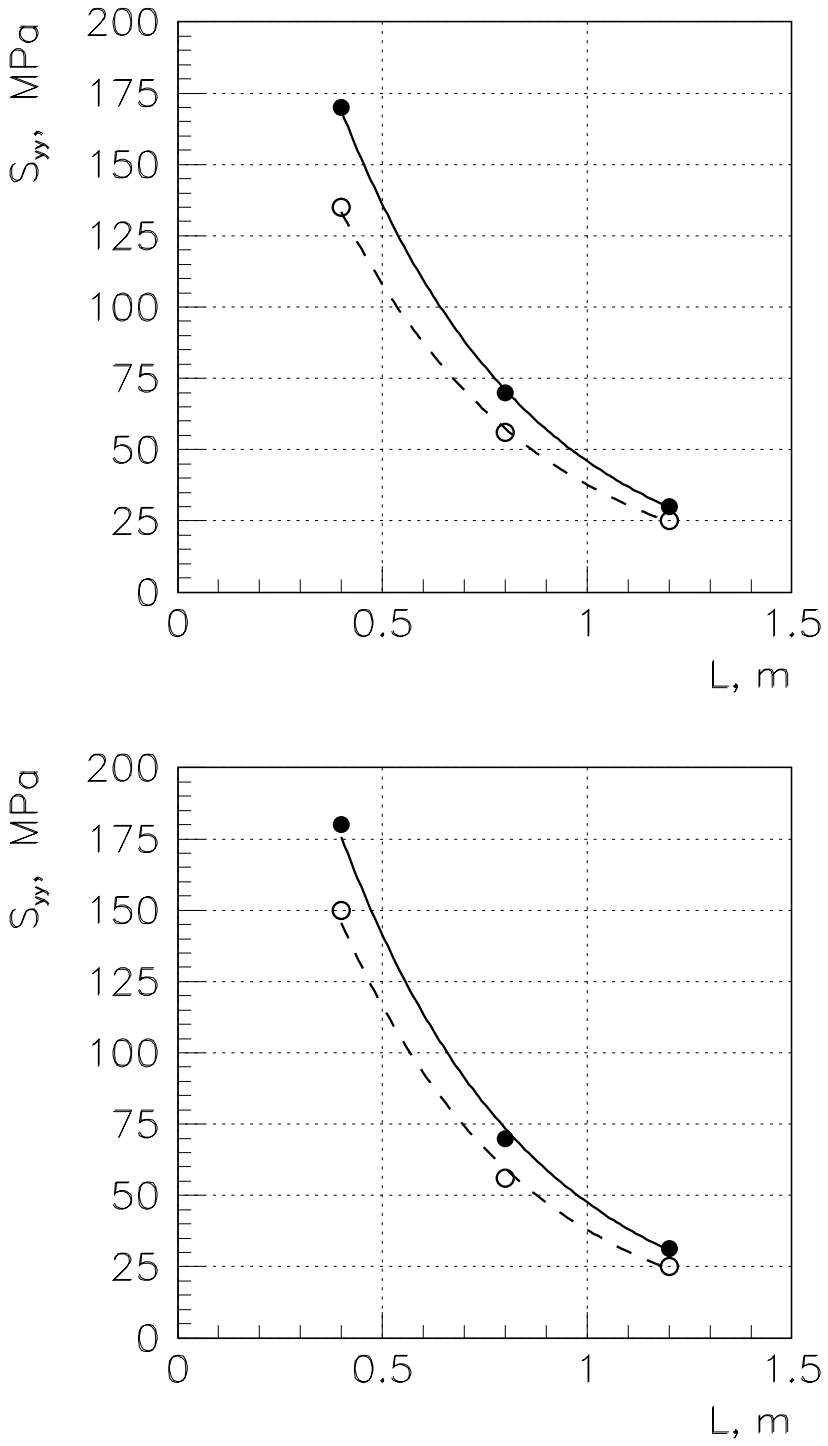

Figure 2.10: Maximum tensile stresses (S_{yy}) on the internal surface of the ceramic insulator as functions of the baffle length in case of the proton beam directions 3 (top) and 4 (bottom). Dashed lines — the plane stress, solid lines — the plane strain.

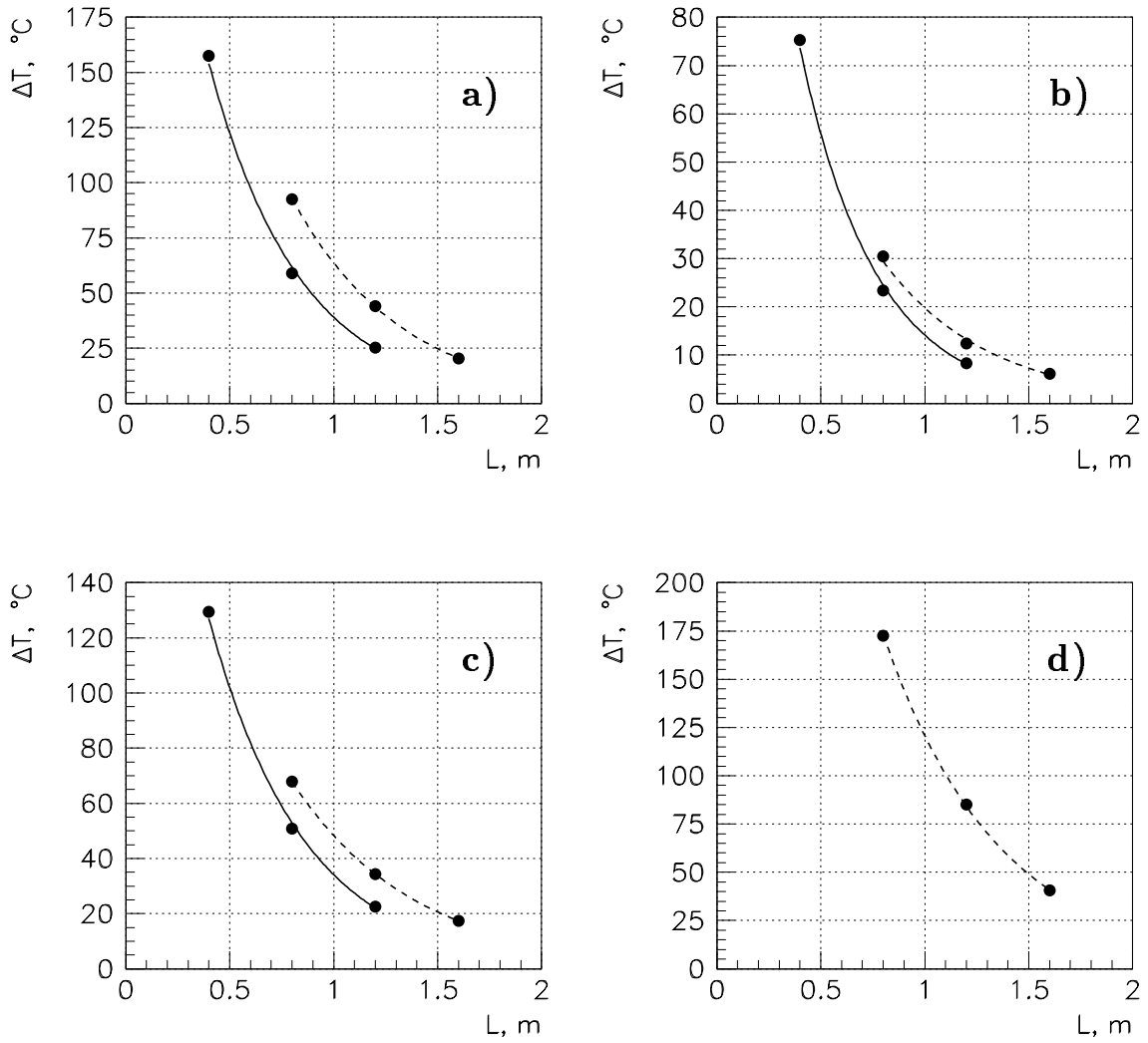

Figure 3.1: Temperature rises for different lengths of the baffle in the cooling pipe steel (a), in the horn neck (b), in the ceramic insulator (c) and in the solder joint between graphite segments and cooling pipe (d). The distance L_{bt} between the downstream end of baffle and the upstream end of target core is equal to 176 cm (solid lines) and 86 cm (dashed lines).

4 Baffle Design

The general view of the baffle collimator, principal dimensions and some details of its design are shown in Figures 4.1–4.3. The baffle core consists of nine 150 mm length graphite rods (or four 300 mm length rods plus one 150 mm length rod). Each rod is machined to needed shape and sizes by means of a grinding machine from ZXF-5Q graphite rods with 57.1 mm diameter inventory size. The hole for the beam passage is machined by means of a circular grinding machine.

Graphite rods are encapsulated into a metal (aluminum) casing, which has a good thermal contact with graphite, provides an integrity of design and prevents eroding of a lateral side (the cooling surface) of graphite rods by an air flow. Encapsulation is provided with help of a zone-normalized deformation method including the following stages:

- graphite rods are placed inside the aluminum pipe with a small gap equal to 0.05–0.1 mm;
- the aluminum pipe is stretched in the longitudinal direction and heated locally to the temperature about 400°C with help of the circular electron beam gun moving along the pipe axis;
- to provide an uniform azimuthal heating, the pipe is rotated around its axis.

At the stage of cooling the aluminum pipe shrinks plastically. Its relative lengthening may be estimated as

$$\Delta(2\pi R)/2\pi R = (\alpha_{al} - \alpha_g)\Delta T \simeq 0.006,$$

where $\alpha_{al} = 24.5 \times 10^{-6}$ K^{-1} and $\alpha_g = 8.9 \times 10^{-6}$ K^{-1} are the average coefficients of thermal expansion of aluminum and graphite, respectively, in a temperature range 20–400°C, $R = 28.5$ mm is the baffle radius and $\Delta T \simeq$ 380°C. This relative lengthening is three times larger than the permanent deformation at the yield strength S_{02}. It means that the final tensile stress in the aluminum pipe will be practically equal to the yield strength and, as a result, the pressure applied to the graphite from the side of aluminum pipe (the shrinking pressure) will be equal to $P \simeq \frac{a}{R} S_{02}$, where $a = 2$ mm

is the thickness of pipe. For deformable Russian aluminum alloys AMg2M–AMg6M the yield strength lies in a range 100–170 MPa and, by this means, the shrinking pressure varies from 7 MPa up to 12 MPa.

The baffle design includes two beryllium windows to prevent eroding of graphite rods along their internal surface. In order to refuse from additional flanges, which will increase essentially the total length of the baffle collimator, beryllium window is pressed to the graphite via stainless steel ring by means of rolling of the aluminum pipe ends.

Two channels (Figure 4.3, view B and D) are used for ventilation of the baffle internal volume.

The temperature of the external surface of baffle is monitoring with help of four thermocouples, which are mounted as it is shown in Figure 4.3 (section C-C and view A). The thermocouple applied in this design is a chromel-alumel thermocouple type KTXA04.06 of TESEY company (Obninsk, Kaluga region, Russia). This type of thermocouple has a time constant $\tau \simeq 0.8$ s, i.e. a very fast response to the temperature change.

Series of six pin-balls will provide the proper alignment of baffle into the beam line.

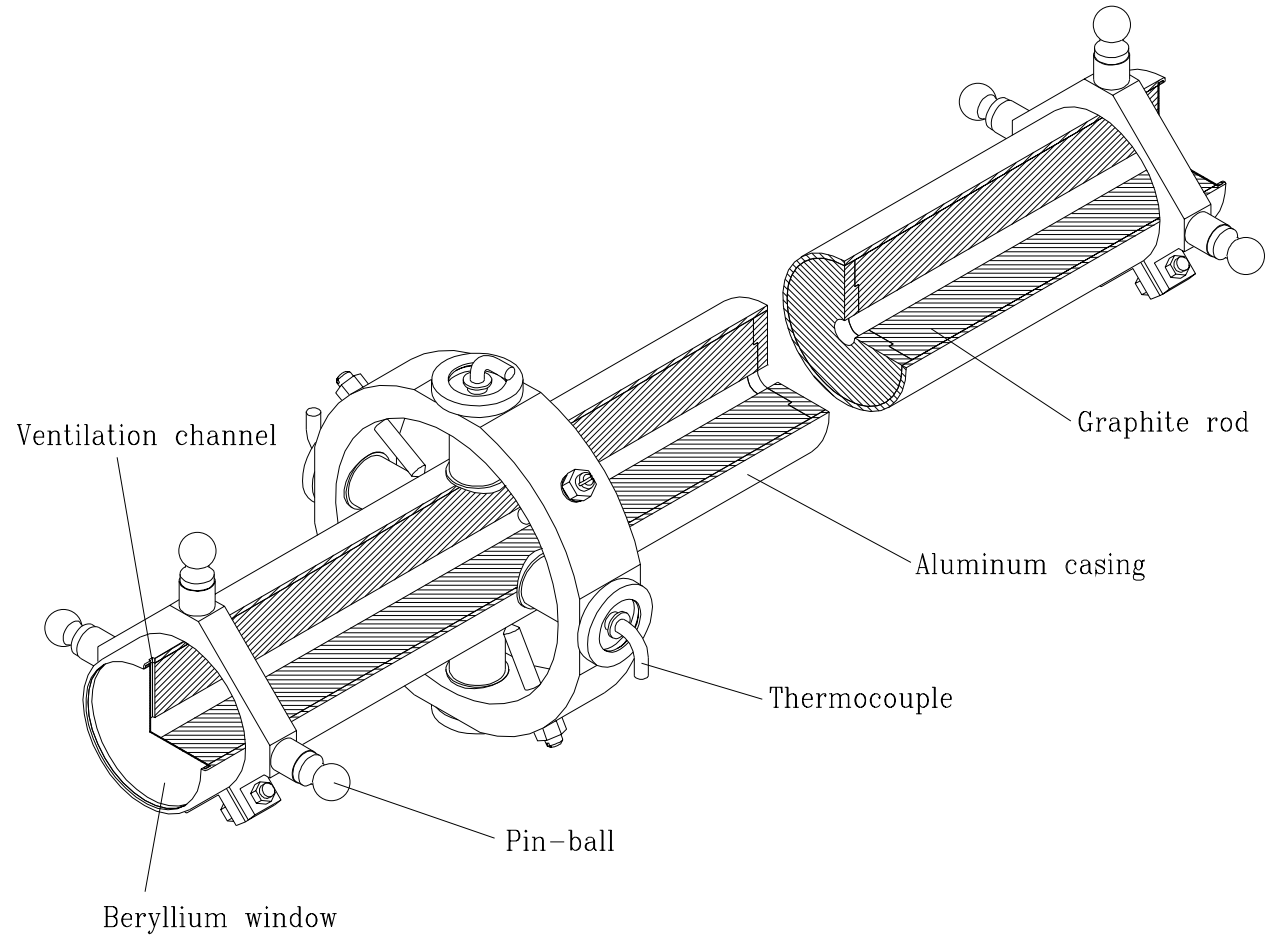

Figure 4.1: General view of the baffle collimator.

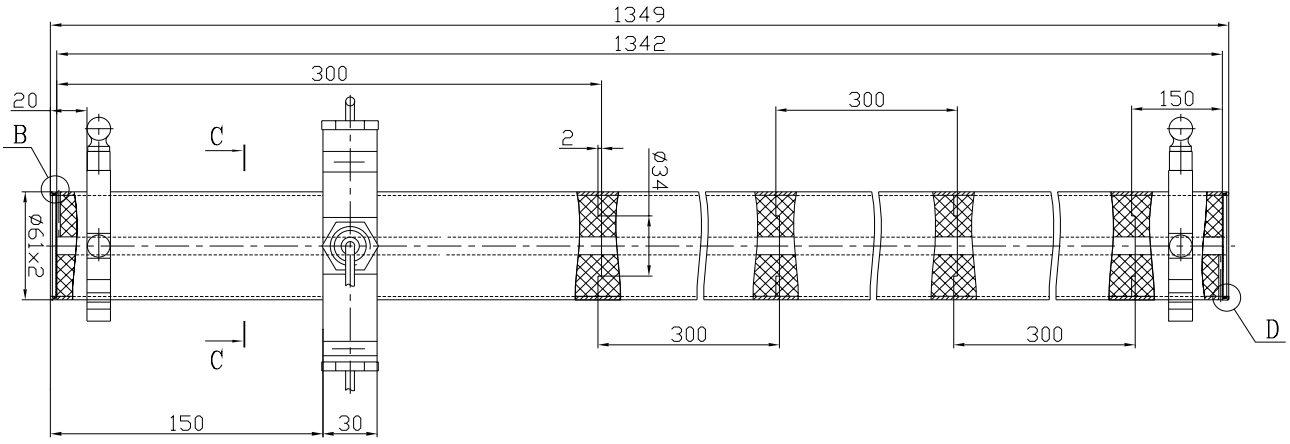

Figure 4.2: Principal dimensions of the baffle collimator.

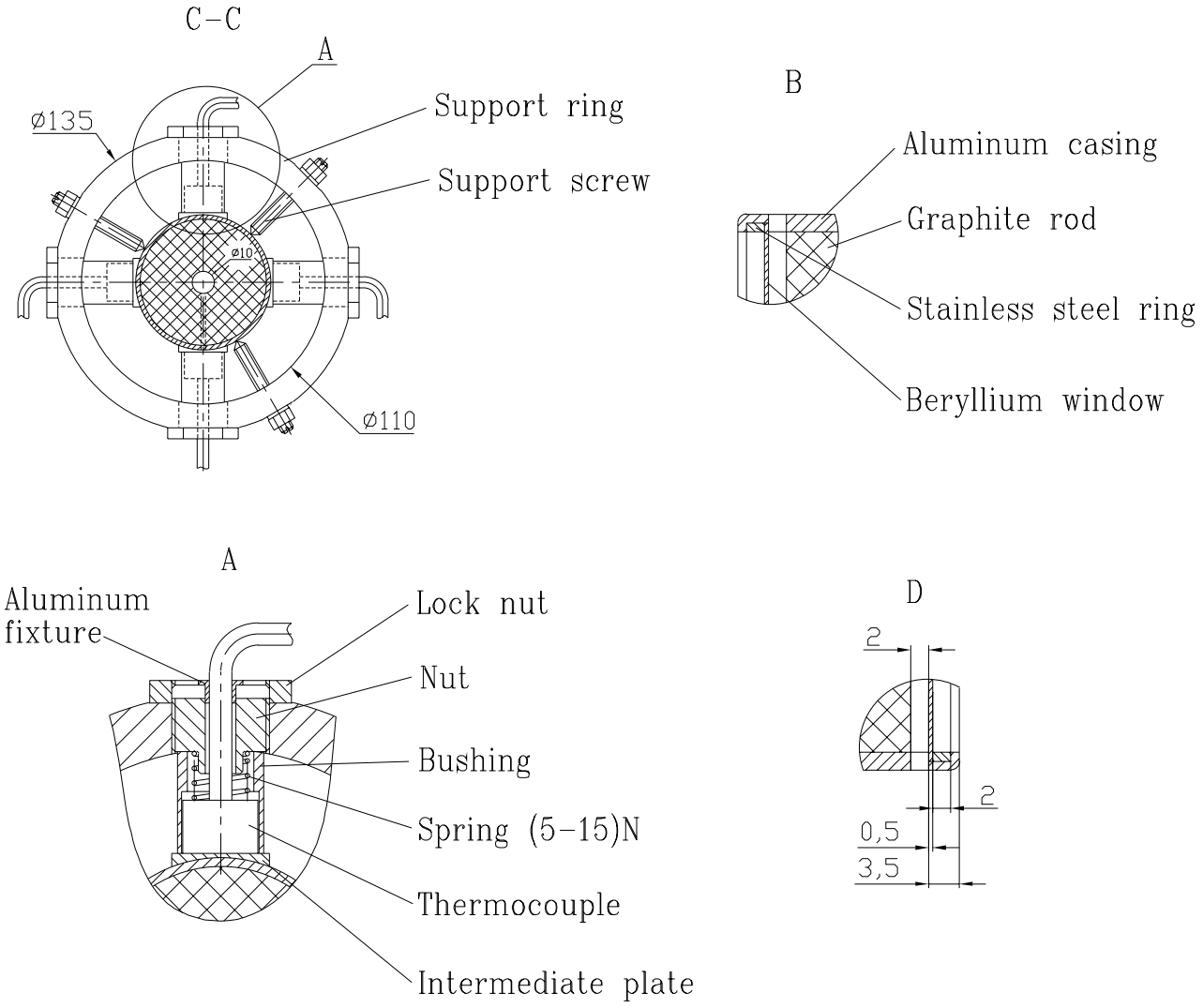

Figure 4.3: Some details of the baffle design.

5 Normal Operational Mode

The results of MARS calculations of deposited power in the graphite core and in the aluminum casing for 1% proton tail hitting the baffle are shown in Figure 5.1. The deposited power reaches its maximum value about 17.3 W per 7.5 cm length bin at the downstream end of baffle.

5.1 Convection Coefficients for the Air Cooling of Baffle

For an air cooling of baffle the convection coefficient α was calculated using the following formula [4]:

$$\alpha = \frac{Nu}{d}\lambda(1 - 0.54\cos^2\varphi),$$

where Nu is the Nusselet number, λ is the air heat conductivity, d is the baffle diameter, $\varphi = \pi/2$ for the transverse cooling and $\varphi = 0$ for the longitudinal cooling. The Nusselet number Nu was calculated using empirical relation:

$$Nu = ARe^m Pr^{0.33}.$$

Coefficients A and m depend on Reynolds number $Re = vd/\nu$, where ν is the air viscosity and v is the air flow velocity. For the air flow velocity range from 1 up to 15 m/s Reynolds number is $4 \times 10^3 \leq Re \leq 6 \times 10^4$, thus $A = 0.22$ and $m = 0.6$ [4].

The dependence of convection coefficient on the air flow velocity for the transverse and longitudinal cooling is shown in Figure 5.2. At the air flow velocity about 4.4 m/sec (this value of an air flow velocity is specified in [5]) the convection coefficient lies in the range from 12 up to 28 W/m^2/K depending on the direction of the air flow with respect to the baffle axis. Therefore, calculations of the baffle temperature have been made for convection coefficients 12, 20 and 28 W/m^2/K.

5.2 Baffle Temperature

Supposing that the cooling of baffle is produced by the air convection on its lateral side with the convection coefficient α, the temperature distribution along the baffle may be defined solving the equation of thermo-conductivity,

which can be written as follows:

$$\frac{d^2T(z)}{dz^2} = \frac{2\alpha T(z)}{\lambda R} - \frac{Q(z)}{\lambda},$$

where $T(z)$ is the difference between the baffle temperature and the ambient temperature, λ is the thermal conductivity of graphite, R is the baffle radius, $Q(z)$ is the volume density of deposited power. In our calculations we supposed that $Q(z)$ is defined by the sum of deposited power in graphite and aluminum and the external radius of graphite is equal to 30.5 mm.

Given above equation was solved by the fourth order Runge-Kutta method with boundary conditions $dT(z)/dz = 0$ at $z = 0$ and $z = L$, where L is the baffle length. The main difficulty in solving of this equation is the unknown temperature $T(0)$. This temperature was defined by the method of successive approaches to satisfy $dT(z)/dz = 0$ at $z = L$ and

$$\int_0^L \alpha 2\pi R T(z) dz = P_t,$$

where P_t is the total power deposited in a baffle.

Results of these calculations of the baffle temperature for different convection coefficients α are given in Figure 5.3 in comparison with results of ANSYS calculations, which were made taking into account the deposited power in aluminum and graphite separately. The ambient temperature was taken equal to 16°C. Due to a good accuracy of analytical calculations they may be used for quick estimations of temperature for different initial conditions (deposited power, baffle sizes, convection coefficients).

As it follows from Figure 5.3, the maximum temperature of baffle does not exceed of 107°C even in the hardest case, when the direction of the air flow is parallel to the baffle axis. As the direction of air flow is unknown, the maximum temperature of the baffle should lie in a range 60–107°C and there is no need in a water cooling of baffle.

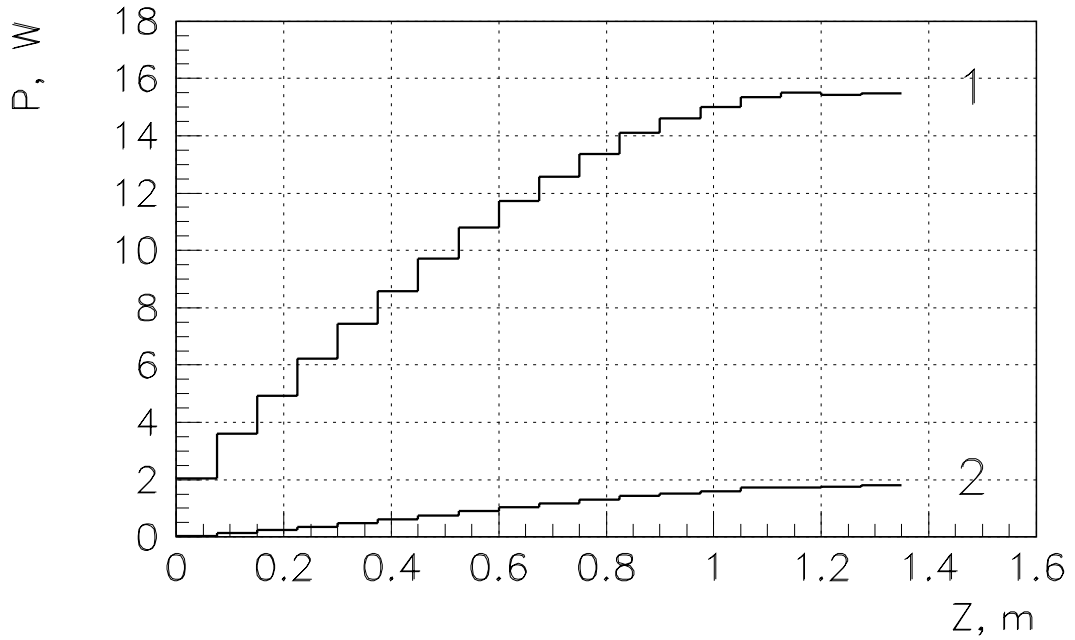

Figure 5.1. Distributions of deposited power along the baffle for 1% beam tail hitting the graphite: 1 – graphite, 2 – aluminum casing.

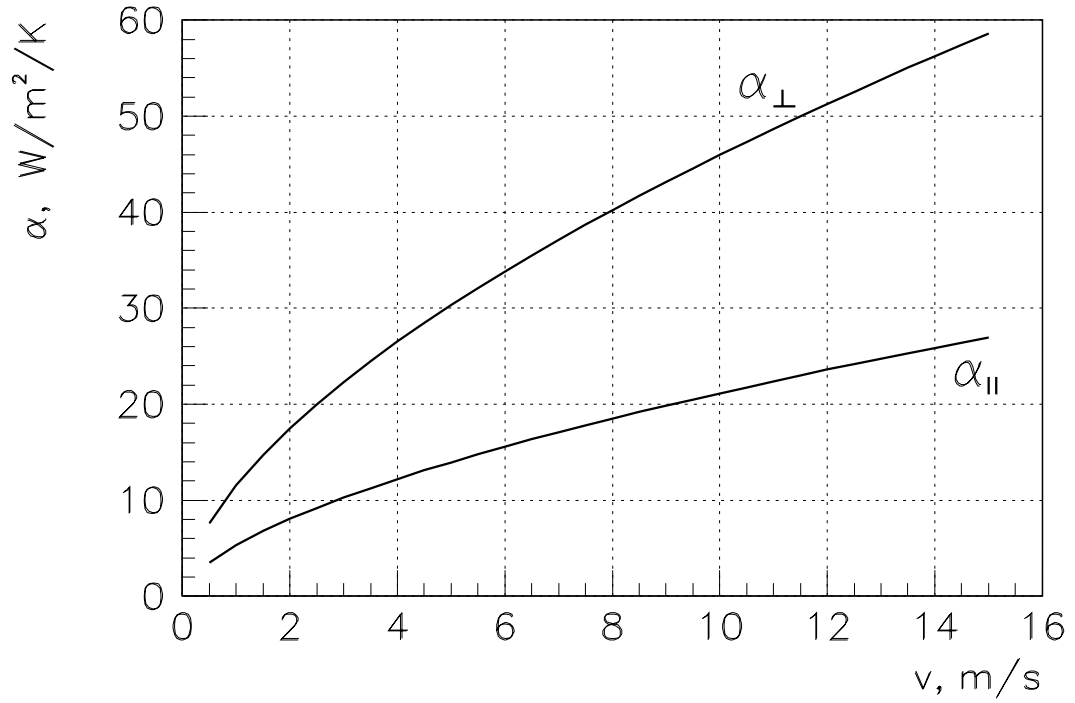

Figure 5.2. Convection coefficients as functions of the air flow velocity: $\alpha_{\perp}$ – the direction of air flow is perpendicular to the baffle axis, $\alpha_{||}$ – the direction of air flow is parallel to the baffle axis.

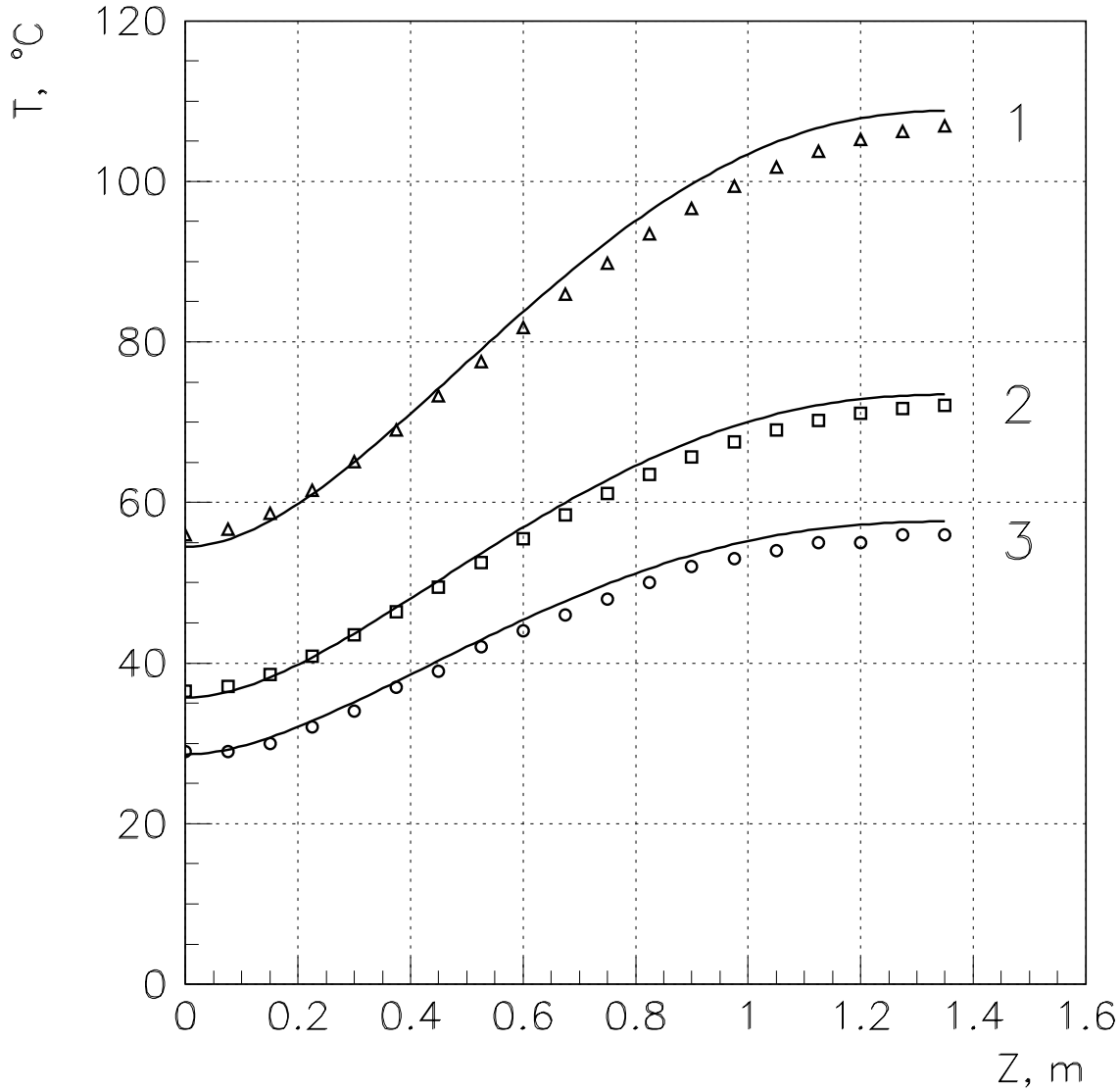

Figure 5.3. Temperature distributions along the baffle. Solid lines and points give results of analytical and ANSYS calculations, respectively. Numbers correspond to different convection coefficients: 1 — 12 W/m^2/K, 2 — 20 W/m^2/K, 3 — 28 W/m^2/K.

6 Emergency Mode

In a case of emergency the full intensity proton beam will hit the baffle. The transverse distribution of proton beam and corresponding distribution of an energy deposition density in the baffle core were taken the same as for calculations of the graphite target. Calculations of temperature and stresses in a baffle were made with help of ANSYS.

6.1 Maximum Baffle Temperature

The maximum temperature of graphite defines its operational environment: neutral gas, vacuum or air. It is connected with oxidation of graphite at the high temperature. Poco Graphite Inc. specifies, that the oxidation of graphite by oxygen (as well as other gases) is highly temperature dependent, but no detectable reaction occurs at the temperature below 350°C. Graphite oxidation is characterized by an oxidation threshold. It is the temperature that results in 1% weight loss in 24 hours. For the ZXF-5Q grade this temperature is equal to 450°C.

Distribution of the baffle temperature after one emergency spill in the case when the center of proton beam is located at $x_b = 5$ mm is shown in Figure 6.1. Evolution of temperature in time at the point located 15 cm from the upstream end of a baffle, where the density of energy deposition has a maximum value, is shown in Figure 6.2. Calculations were made for the minimum value of convection coefficient 12 W/m^2/K. As it follows from this Figure, the maximum temperature does not exceed 344°C, moreover the velocity of its drop is so high (ANSYS calculations give 10°C/ms) that it will exists only a few ms. Taking into account that emergency should continue only a few beam spills, it can not lead to the noticeable oxidation of graphite. Therefore, the baffle core can be exposed to air.

6.2 Temperature Monitoring

The evolution of temperature in time for 7 emergency beam spills in different points, located at the baffle surface, is shown in Figure 6.3 for the proton beam position $x_b = 5$ mm. The temperature rise after the first spill reaches the value of ~1.2°C in the nearest to beam location point (point 1 in our case). Temperature rises in points 2 and 3 are essentially lower. It means, that using of four thermocouples located ~15–30 cm from the upstream end of baffle (the cross-section with the maximum energy depo-

sition density) will allow to detect the emergency situation in one or two beam spills. In addition, an asymmetry of thermocouple signals may be used to monitor the position of mis-steered proton beam.

In order to detect an increase of temperature with sufficient resolution, the used thermocouples should have a fast response to the temperature rise. The response F of thermocouple to the 1°C temperature jump as a function of the thermocouple time constant τ is $F(\tau) = 1 - \exp(-T_0/\tau)$, where T_0 is the repetition period. Figure 6.4 shows that for $T_0 = 1.9$ s the use of thermocouples with a time constant $\tau = 2.7$ s leads to the 50% loss of thermocouple signal. It is evidently, that besides of proposed above thermocouples, another types of thermocouples with a time constant ~1–2 s may be used for temperature monitoring. The low value of time constant is essential also in the case of their using for the primary beam alignment with a beam scan.

6.3 Stresses in the Baffle

The stresses arising in the baffle core due to full intensity beam hitting were calculated for three locations of proton beam axis: $x_b = 5, 10, 15$ mm. ANSYS calculations show that stresses in the baffle core does not depend on the baffle length if the length is greater than 10 cm. Therefore calculations of stresses were made for the 20 cm length graphite rod under the following boundary conditions:

- graphite is exposed to external pressure of 10 MPa on its lateral side;
- the ends of rod are free to the movement.

The maximum equivalent stress of 42.8 MPa arises in the case of $x_b =$ 5 mm, i.e. when only the half of the beam hits the baffle (Figure 6.5). One should note, that in the region of proton beam graphite is exposed of all-axis compression, what is illustrated in Figure 6.6-6.8 where distributions of three principal stresses are shown. The ultimate compressive strength of ZXF-5Q graphite is equal to 195 MPa and the high cycle fatigue limit may be estimated as $\sim 0.4 \times 195 = 78$ MPa. It means that the baffle core will not lose its integrity even in terms of high cycle fatigue. Nevertheless, the surface of hole in baffle should be machined without strength losses.

The similar situation takes place for other locations of the proton beam axis ($x_b = 10$ mm and $x_b = 15$ mm), but stresses in these cases are essentially lower than for $x_b = 5$ mm (25.9 MPa and 23.8 MPa, respectively).

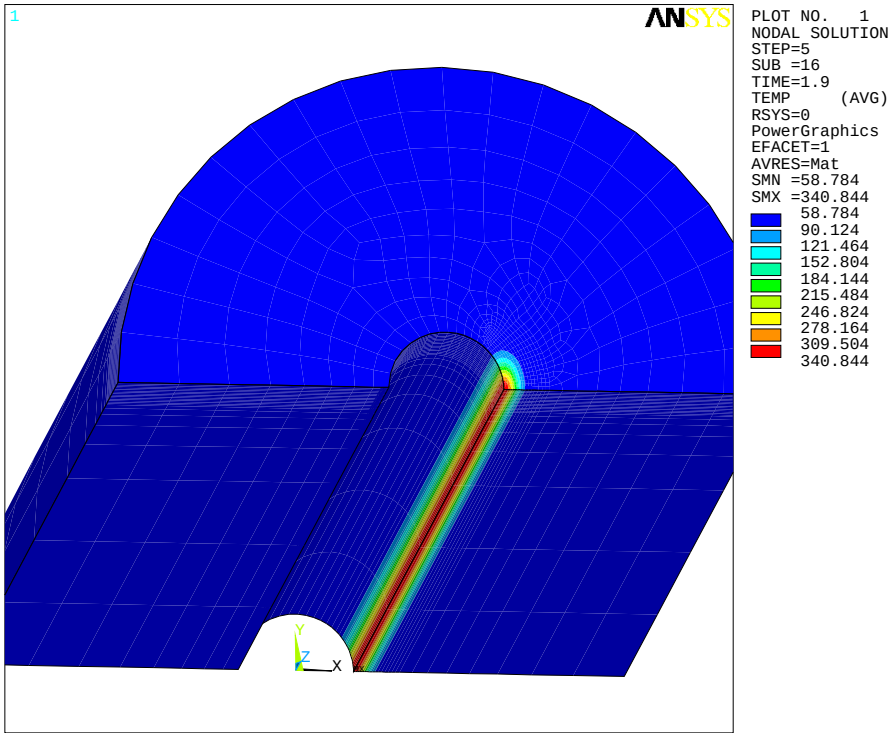

Figure 6.1 (colour): Distribution of temperature after one emergency spill with $x_b = 5$ mm.

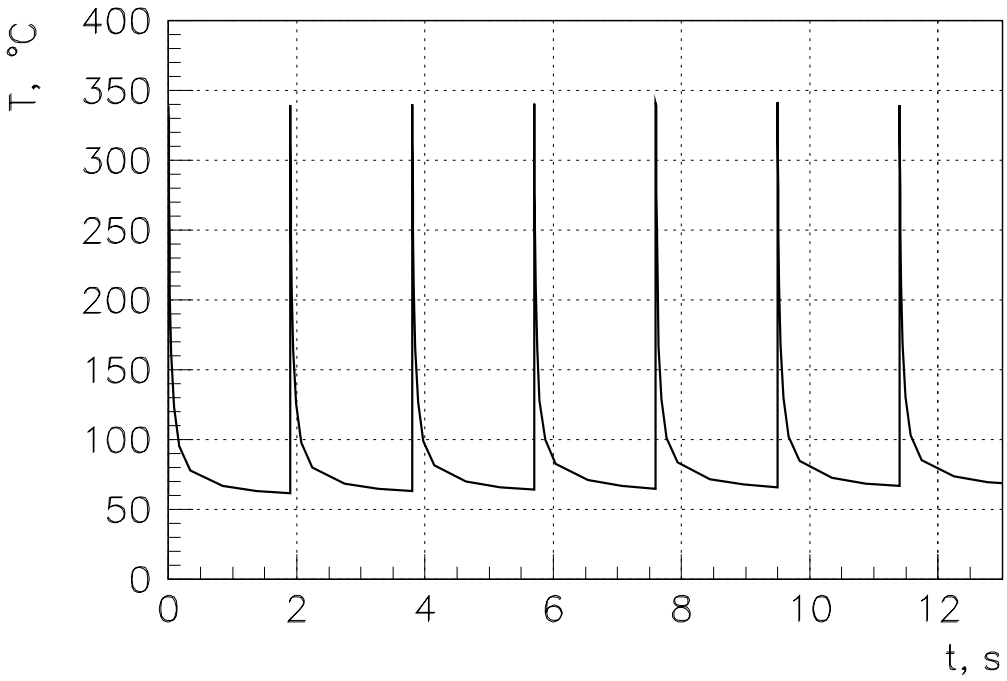

Figure 6.2. Time evolution of temperature at the beam axis during seven emergency spills after steady state at the normal operation mode.

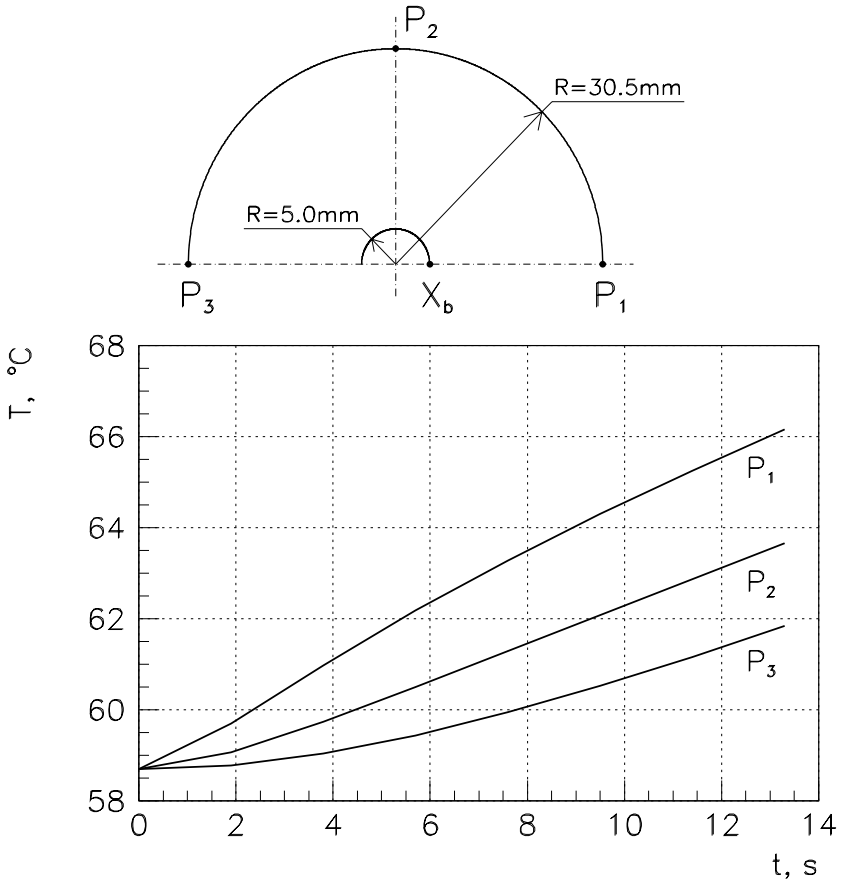

Figure 6.3. Time evolution of temperature in different points on the baffle surface during seven emergency spills with $x_b = 5$ mm.

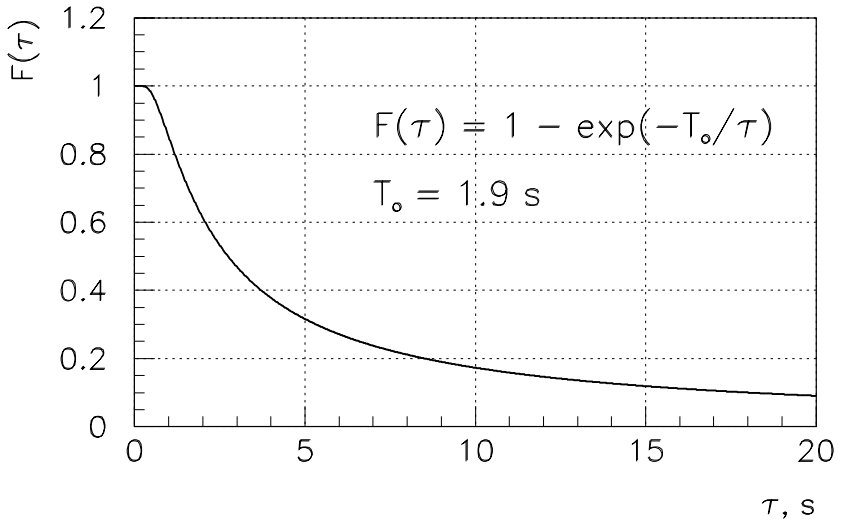

Figure 6.4. Response of thermocouple to 1°C jump as a function of its time constant.

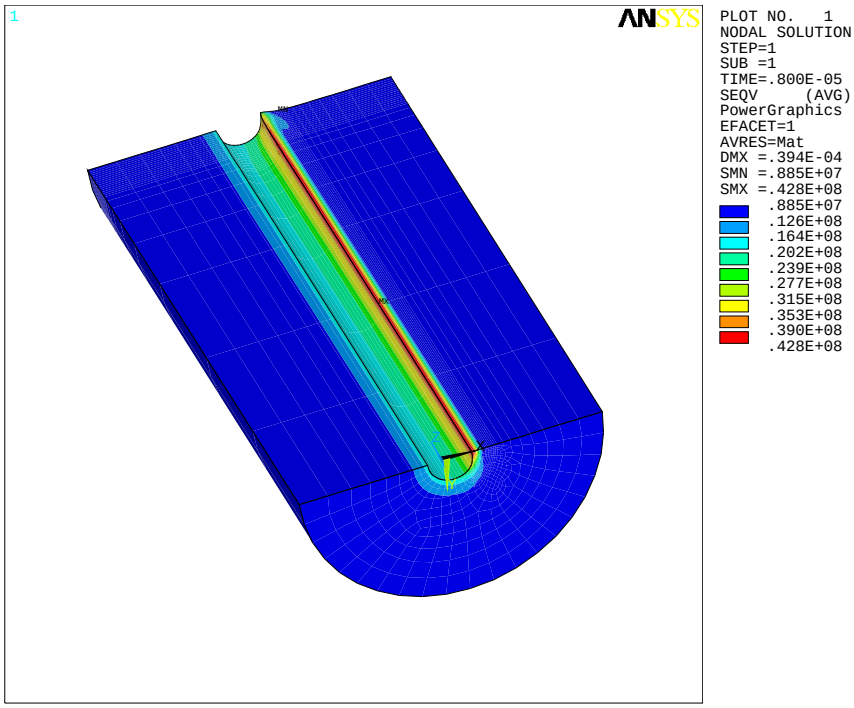

Figure 6.5 (colour): Distribution of equivalent stress after one emergency spill with $x_b = 5$ mm.

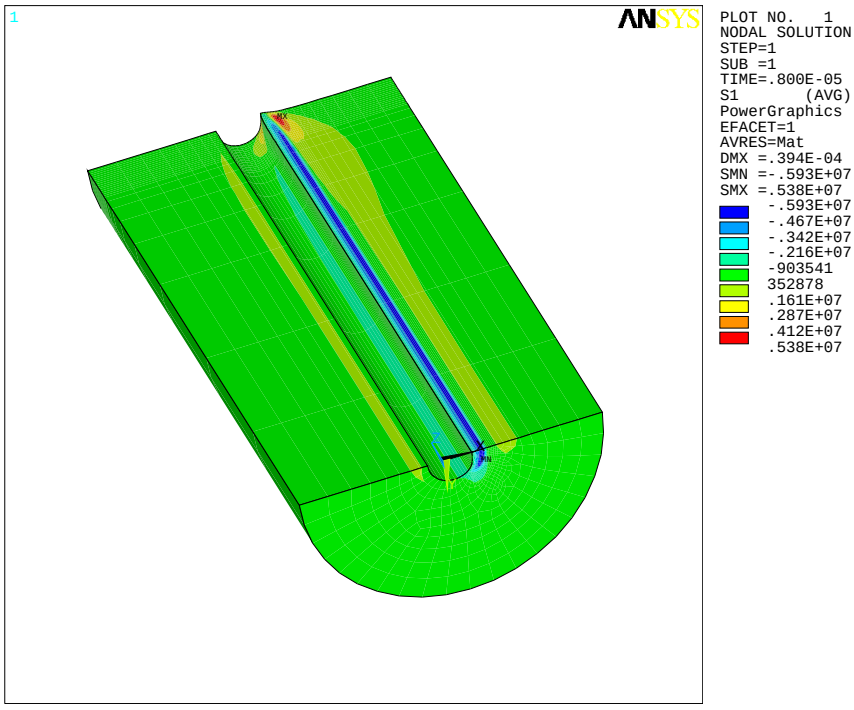

Figure 6.6 (colour): Distribution of principal stress S1 after one emergency spill with $x_b = 5$ mm.

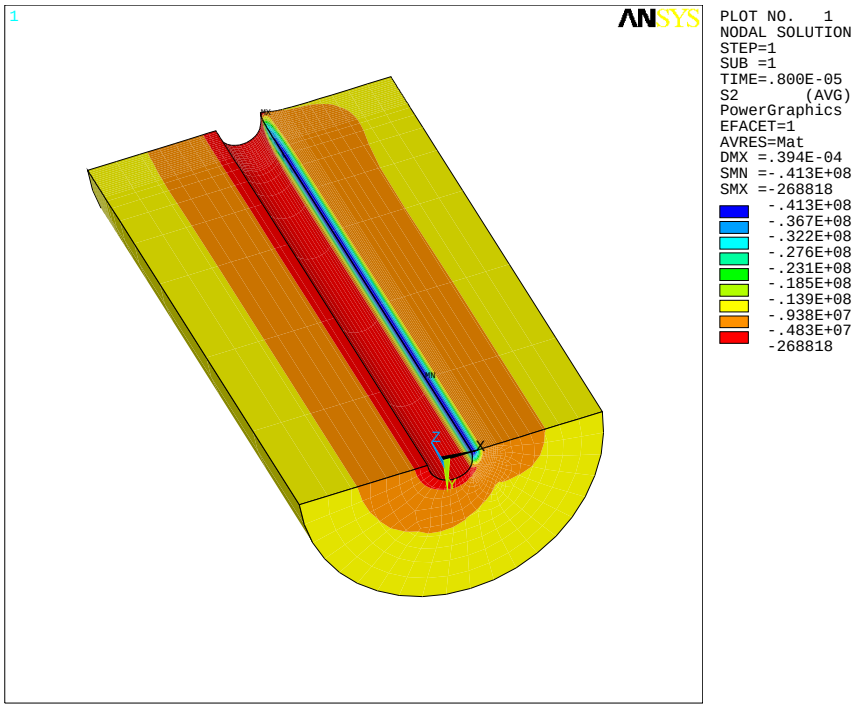

Figure 6.7 (colour): Distribution of principal stress S2 after one emergency spill with $x_b = 5$ mm.

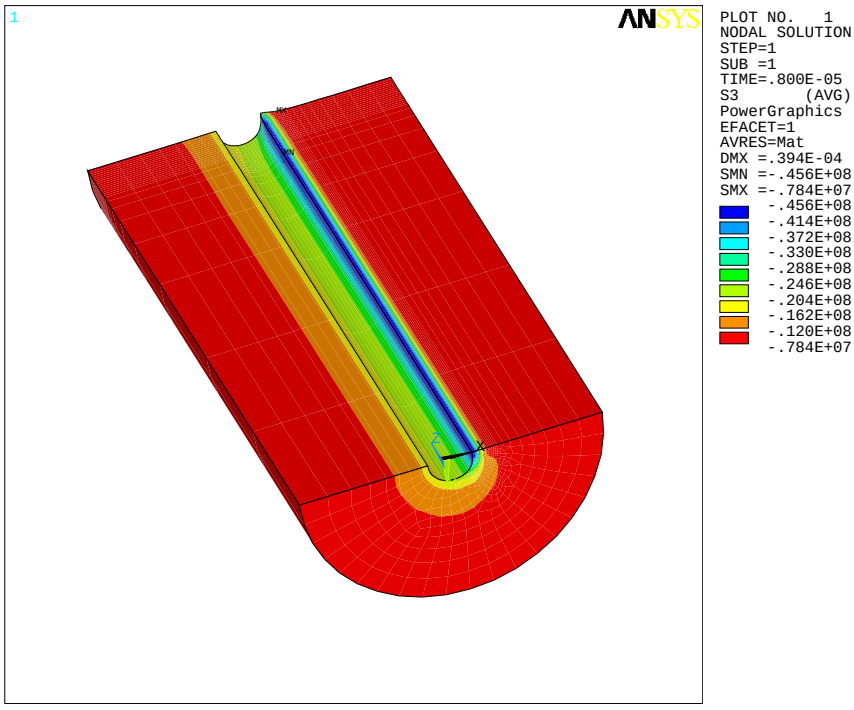

Figure 6.8 (colour): Distribution of principal stress S3 after one emergency spill with $x_b = 5$ mm.

7 Conclusions

Considered above design of the baffle collimator showed that:

- the baffle collimator with a length of 120 cm at $L_{bt} = 176$ cm or 135 cm at $L_{bt} = 86$ cm (L_{bt} is the space between the downstream end of baffle and the upstream end of target) will provides a quite reliable protection from failure in case of the mis-steered proton beam even for the weakest parts of target and horn;
- for 1% of proton beam tail hitting the baffle at normal operation mode the quite reliable temperatures are achieved even for air cooling on the lateral side of baffle casing;
- the graphite baffle core may be exposed to air. There is no need in inert gas or vacuum;
- the baffle temperature should be monitored by means of at least four thermocouples;
- the maximum equivalent stress arising in a baffle in the case of emergency does not exceed of 42.8 MPa, that can not lead to the baffle failure.

At the stage of baffle design the possibility of encapsulation of graphite rods into aluminum pipe was investigated by means of construction of the 45 cm length baffle prototype. Three 58 mm diameter and 150 mm length graphite rods were encapsulated into 62 mm diameter aluminum pipe with 1.5 mm wall thickness (Russian aluminum alloy AMg2M) with help of a zone-normalized deformation method. Photos of baffle prototype are given in Figure 7.1. Construction of 45 cm length prototype confirms the reliability of the proposed baffle design.

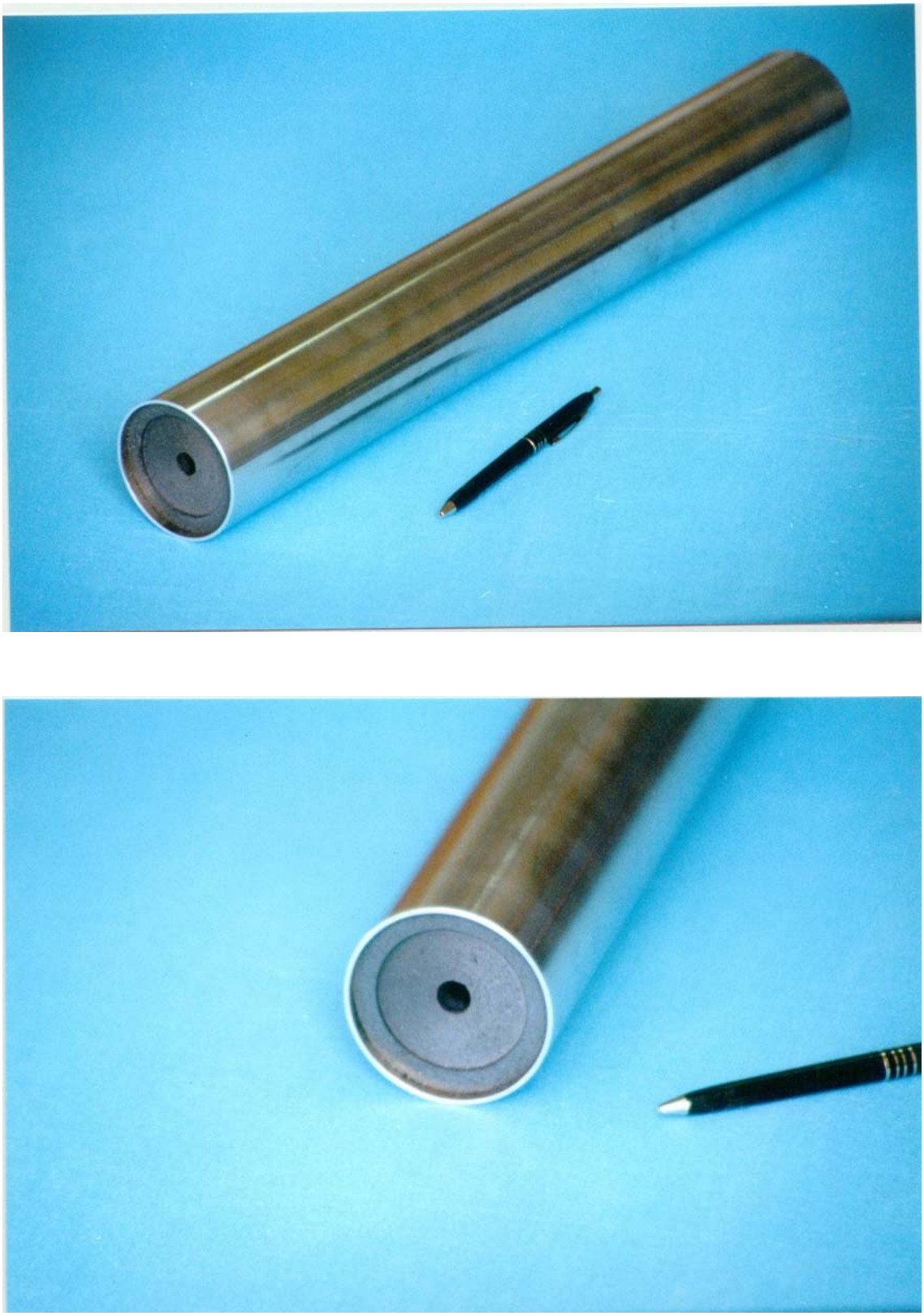

Figure 7.1 (colour): The 45 cm length prototype of baffle collimator.

References

[1] I.Azhgirey et al., Proceedings of XV Workshop on Charged Particles Accelerators, v.2, p.270, Protvino, 1996.

[2] A.Abramov, S.Filippov, N.Galyaev et al. Dynamic Stress Calculations for ME and LE Targets and Results of Prototyping for the LE Target, Protvino, 2000, NuMI-B-675.

[3] The NuMI Facility Technical Design Report, Fermilab, 1998.

[4] V.A.Grigoriev, V.M.Zorin, Theoretical Aspects of Heat-technique. Heat-technique Experiment, V.2, Handbook, Energoatomizdat, Moscow, 1988.

[5] Hylen's e-mail from February 9, 2002.